Article:
Otitoju, O., Oko, E. and Wang, M. orcid.org/0000-0001-9752-270X (2023) Modelling, scale-up and techno-economic assessment of rotating packed bed absorber for CO2 capture from a 250 MWe combined cycle gas turbine power plant. Applied Energy, 335. 120747. ISSN 0306-2619

https://doi.org/10.1016/j.apenergy.2023.120747

Applied Energy 335 (2023) 120747

Contents lists available at ScienceDirect

Applied Energy

journal homepage: www.elsevier.com/locate/apenergy

Modelling, scale-up and techno-economic assessment of rotating packed bed absorber for CO_2 capture from a 250 MW_e combined cycle gas turbine power plant

Olajide Otitoju [a], Eni Oko [b], Meihong Wang [a,*]

[a] Department of Chemical and Biological Engineering, University of Sheffield, Sheffield S1 3JD, United Kingdom
[b] School of Engineering, Newcastle University, Newcastle upon Tyne, NE1 7RU, United Kingdom

HIGHLIGHTS

- Rate-based model of a monoethanolamine-based rotating packed bed absorber was developed and validated at a pilot scale in Aspen Custom Modeller.
- RPB absorber model scaled up using a newly proposed iterative scale procedure.
- Technical and economic assessments analysis were performed.
- Volume reduction factor of 4–13 times was achieved with rotating packed bed absorbers compared to packed bed absorbers.
- Capital expenditures of the rotating packed bed absorbers were lower by 3–53% compared to packed bed absorbers.

GRAPHICAL ABSTRACT

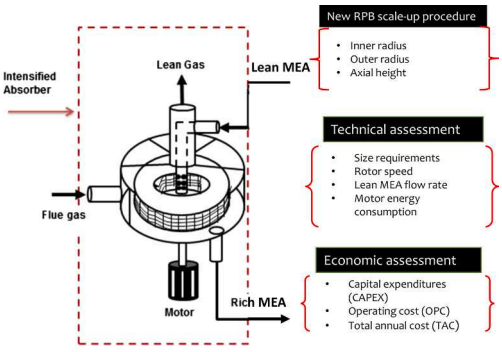

ARTICLE INFO

Keywords:
Post-combustion carbon capture
Chemical absorption
Rotating packed Bed
Scale-up
Technical and economic assessments
Combined cycle gas turbine power plant

ABSTRACT

The huge sizes and costs of the packed bed (PB) absorbers and strippers in solvent-based post-combustion carbon capture are part of the challenges limiting its commercialization. The rotating packed bed (RPB) absorbers and strippers have the potential to reduce the size and cost of the CO_2 capture process when used to replace their PB counterparts. However, the size and cost have not been quantified for a large-scale RPB. Therefore, this paper is devoted to providing detailed technical and economic assessments of a large-scale RPB absorber operated with concentrated (55-75 wt%) monoethanoamine (MEA). To achieve this, a steady-state rate-based model of the RPB absorber was developed and validated in Aspen Custom Modeller®. The model was scaled up to capture CO_2 from the flue gas of a 250 MW_e CCGT power plant using an iterative scale-up methodology proposed in this study. Technical assessments of the large-scale RPB absorber indicated that a 4–11 times volume reduction factor was achieved with 55 wt% MEA concentration compared to PB absorbers. The highest volume reduction factors of 5–13 times were achieved in RPB absorber operated with 75 wt% MEA. Economic assessments show that the

Abbreviations: ACM, Aspen Custom Modeller; CCGT, Combined Cycle Gas Turbine; MEA, Monoethanolamine; PB, Packed Bed; PCC, Post-combustion Carbon Capture; RPB, Rotating packed Bed; RPM, Rotation per minute.

* Corresponding author.
E-mail address: Meihong.Wang@sheffield.ac.uk (M. Wang).

https://doi.org/10.1016/j.apenergy.2023.120747
Received 24 August 2022; Received in revised form 18 January 2023; Accepted 20 January 2023
Available online 2 February 2023

capital expenditures of the RPB absorbers were lower by 3–53%. The CO_2 capture cost was also lower ($6.5/$t_{CO2}$–$9/t_{CO2}) compared to $15/$t_{CO2}$–$24/t_{CO2} obtained for the PB absorbers.

Nomenclature

A_c	Cross-sectional area of the RPB (m^2) = $2\pi r$ for RPB
a_{gl}	Gas-liquid interfacial area (m^2/m^3)
a_t	Specific surface area of packing (m^2/m^3)
$a_p^{'}$	Surface area of the 2 mm diameter bead per unit volume of the bead (1/m) with value 0f 3000 (1/m)
Cl_i	Concentration of component *i* (kmol/m^3)
$C_{p,g}$	Gas-specific heat capacity (kJ/kg K)
$C_{p,l}$	Liquid-specific heat capacity (kJ/kg K)
$D_{g,i}$	Diffusivity of component *i* in the gas phase (m^2/s)
d_h	Hydraulic diameter (m)
$D_{l,i}$	Liquid diffusivity of component *i* (m^2/s)
d_p	Effective diameter of packing (m)
E_i	Enhancement factor of component i
f_d	The fraction of the r_i occupied by the liquid distributor with the value of 0.25–0.33
F_g	Gas molar flow rate (kmol/s)
F_l	Liquid molar flow rate (kmol/s)
G	Mass flow rate of flue gas (kg/s)
g	Acceleration due to gravity (m/s^2)
g_0	Characteristic acceleration with a value of 100 m/s^2
$He_{l,i}$	Henry constant of component i in the liquid (bar.m^3/kmol)
h_{gl}	Interfacial heat transfer coefficient (kW/m^2 K)
$\Delta H_{rxn_{CO_2}}$	Heat of absorption of CO_2 which is 87,000 (kJ/kmol)
$\Delta H_{vap_{,H_2O}}$	Heat of vaporization of water (kJ/kmol)
$\Delta H_{Vap_{H_2O,bp}}$	Heat of vaporization at boiling point (kJ/kmol)
$k_{g,i}$	Mass transfer coefficient of component *i* in the gas phase (m/s)
$k_{l,ave}$	Average liquid film mass transfer coefficient (m/s)
$k_{l,i}$	Mass transfer coefficient of component i in the liquid phase (m/s)
$K_{tot,i}$	Overall gas-phase mass transfer coefficient of component *i* (kmol/m^3 s bar)
L	Mass flow rate of MEA solvent (kg/s)
N_i	Molar transfer fluxes of component i (kmol/m^2.s)
$P_{g,i}$	The partial pressure of component *i* in the gas phase (bar)
P_i^*	Equilibrium partial pressure of component *i* (bar)
P_m	Motor electrical power (kW)
$P^{l/g}$	Ratio of the kinetic energy of liquid to that of the gas with the value of 4
Q_g	Volumetric flow rate of the flue gas (m^3/s)
Q_l	Volumetric flow rate of MEA solvent (m^3/s).
R	Universal gas constant (kJ/kmol.K)
r	Variable radius (m)
r_i	Inner radius (m)
r_o	Outer radius (m)
r_s	Radius of the stationary housing (m)
T	Temperature (^oC)
T_{bp}	Temperature of water at boiling point (K),
T_c	Critical temperature (K)
T_g	Temperature of the gas phase (K)
T_l	Temperature of the liquid phase (K)
u_l	Liquid superficial velocity (m/s)= $u_L = \frac{Q_L}{2\pi rz}$
u_g	Gas superficial velocity (m/s)= $u_L = \frac{Q_G}{2\pi rz}$
U_{jet}	Liquid jet velocity (recommended: 4 to 5 m/s)
$U_{g,fl}$	Gas superficial flooding velocity (m/s)
U_0	characteristics superficial liquid velocity with a value of 0.01 m/s,
V_o	Volume between the outer radius of the bed and the stationary housing (m^3) = $\pi(r_s^2 - r_o^2)z$
V_t	Total volume of the RPB (m^3) = $\pi r_s^2 z$
x_i	Component *i* molar fraction in the liquid phase
x_0	Component mole fraction in the inlet MEA solvent
y_i	Component *i* molar fraction in the gas phase
y_0	Component mole fraction in the inlet flue gas
y_1	Mole fraction of CO_2 in the inlet gas stream
y_2	Mole fraction of CO_2 in the outlet gas streams.
y_e	Mole fraction of CO_2 in equilibrium with CO_2 concentration in the liquid.
Z	Axial height of rotor (m)

Greek letters

f	Percentage flooding (%)
γ_i	Activity coefficient of component *i*
ρ_g	Gas density (kg/m^3)
ρ_l	Liquid density (kg/m^3)
σc	Critical surface tension (N/m)
σ	Surface tension (N/m)
μ_g	Gas viscosity (Ns/m^2)
μ_l	Liquid viscosity (Ns/m^2)
ε	Porosity (m^3/m^3)
ε_g	Gas holdup
ε_L	liquid holdup
ω	Rotating speed (rad/s)
λ_l	Thermal conductivity of the liquid (kW/mK)
ν_L	liquid kinematic viscosity
ν_o	Characteristic kinematic viscosity with a value of 10^{-6} m^2/s

Notations for costing

C^{al}	The alloys adds cost
C^{en}	The fan and motor enclosure adds cost
C^{RS}	Higher rotational speed adds cost
C_{trans}	Engine transmission to drive ratio adds cost
C_{L+M}^i	Adds labour and material costs for motor, drive and rotor
$C_{L/M}^i$	Minimizes the addition of labour costs if a special alloy is considered
C_{ref}^{drive}	Reference investment cost for the drive
C_{ref}^{motor}	The reference investment cost for the motor
C_{ref}^{rotor}	The reference investment cost for the rotor
n^{drive}	Actual to reference scaling factor for the drive.
n^{motor}	Actual to reference scaling factor for the motor.
n^{rotor}	Actual to reference scaling factor for the rotor.
P_{ref}^{drive}	Drive reference electrical power (kW)
P_{ref}^{motor}	Motor reference electrical power (kW)
V^{RPB}	RPB liquid capacity and.
V_{ref}^{RPB}	Reference liquid capacity of the RPB

1. Introduction

1.1. Background

The global energy consumption has continued to rise in recent years due to population growth and technological advancement [1]. This has led to an increase in global energy-related CO_2 emissions which reached a total of 31.5 Gigatonnes in 2021 [2]. CO_2 emissions from fossil-fuel-fired power plants are responsible for the majority of energy-related emissions in 2021 [2]. Thus there is a need to intensify the removal of CO_2 from the flue gas stream of these plants. This is because CO_2 is a greenhouse gas with a high contribution to global warming. There are three major technological options for CO_2 capture. They are the pre-combustion capture, the oxy-fuel capture and the post-combustion capture. Among these options, post-combustion carbon capture (PCC) via chemical absorption has been rated as the most promising and matured technology for the decarbonisation of the energy sector [3]. Furthermore, the technology can be easily retrofitted to existing power plants thereby making it the only technology that has been implemented at a commercial scale. However, one major drawback of the PCC process is that the size of the packed bed (PB) used as absorber and stripper in the process is huge [4], and this contributes significantly to plant footprint, costs and process time constant leading to sluggish response characteristics. Despite different strategies (such as vapour recompression, split-flow, absorber intercooling, advanced flash stripper and new solvents) implemented in PB to enhance CO_2 capture and reduce the size and cost of the PCC process, these problems persist. This is due in part to the mass transfer limitation that exists in PB and the difficulty (i.e. high viscosity) in operating PB absorbers and strippers with concentrated MEA. With concentrated MEA, the CO_2 absorption performance could be enhanced and the regeneration energy consumption could be reduced. A rotating packed bed (RPB) can enhance mass transfer and can be operated with concentrated MEA (>55 wt% MEA) [5]. The RPB uses a rotor to create a strong centrifugal acceleration of the vapour-liquid system leading to a droplet flow regime. This enhances the gas–liquid interfacial area and the mass transfer rate thus, significantly reducing the packing volume (size) requirement.

1.2. Literature review

The RPB technology has been increasingly used for CO_2 capture and many studies have reported on its application in solvent-based PCC process [5–10]. For instance, Joel et al. [8] developed a rate-based model for an MEA-based RPB absorber using Aspen Plus® and Fortran®. The model was used to investigate the effects of rotor speed, lean MEA concentrations and lean MEA inlet temperature on the CO_2 absorption performance. They found that the volume of the absorber was reduced by 12 times with RPB compared to PB. Kang et al. [11] Investigated the effects of different combinations of mass transfer correlations and liquid holdups on model predictions of CO_2 mole fraction, overall volumetric mass-transfer coefficient of the gas phase and CO_2 removal using an MEA-based RPB absorber model developed in gPROMS®.

The process design of an MEA-based RPB absorber to achieve different CO_2 capture levels (i.e. 80%, 90%, 95% and 99%) using Aspen advanced custom model was reported by Thiels et al. [12]. The authors reported that the packing volume can be reduced by using a series arrangement of RPB and PB for the CO_2 capture process. A summary of the literature review on the modelling and simulation of CO_2 capture in MEA-based RPB absorbers is presented in Table 1.

The modelling of the RPB is different from that of the PB for two reasons: (I) In PB, the mass transfer occurs along the packing only whereas in RPB, an additional zone of mass transfer exists between the rotor and the casing. (II) The PB is a straight bed where absorption takes place under gravity and the gas and liquid mass transfer coefficients do not change due to the constant flow rates of the gas and liquid through the bed. In contrast, the RPB is a tapered bed (Fig. 1) where absorption takes place at high gravity and the varied cross-sectional area of flow along the radial direction leads to variation in the gas and liquid velocities and ultimately variation in gas and liquid mass transfer coefficients [16]. Aspen Custom modeller® (ACM) is a modelling platform that allows the model of the RPB to be developed by taking into account the differences listed above. ACM aids the quick development and simulation of custom process models. Its models can be run in steady state, dynamic, parameter estimation and optimization modes. Its advantage over other modelling platforms includes easy integration with the Aspen Properties database. It also allows for custom procedures to be developed to suit the user's needs. Custom Models developed in

Table 1
Summary of literature review on modelling and simulation of CO_2 capture in MEA-based RPB absorber.

Reference	Simulation tool	Component	Model complexity	Model validation	Description & model application
Joel et al. [13]	Aspen Plus® and Fortran	Absorber	Rate-based mass transfer, chemical equilibrium and reaction kinetics	Steady-state model validation with experimental data by Jassim et al. [6].	• Used two sets of mass transfer correlations to investigate the model prediction's performance against experimental data. Process analysis to study the effects of fixed RPB size, fixed lean MEA flowrates, higher lean MEA temperature and higher flue gas temperature on CO_2 capture level.
Borhani et al. [14]	gPROMS® and Aspen Properties	Absorber	Rate-based mass transfer, chemical equilibrium and enhancement factor	Steady-state model validation with experimental data by Jassim et al. [6].	• Examined the effect of different reaction kinetics and enhancement factors on the CO_2 capture level. Process analysis to evaluate the effect of rotor speed, lean MEA concentration, lean MEA flow rate and lean MEA temperature on the CO_2 capture level.
Oko et al. [5]	gPROMS® and Aspen Properties	Absorber	Rate-based mass transfer, chemical equilibrium and enhancement factor	Steady-state model validation with experimental data by Jassim et al. [6]	• Analysis to evaluate the impact of temperature rise on the liquid phase speciation, equilibrium partial pressure and mass transfer resistance. Proposed different design options for RPB absorber intercoolers.
Oko et al. [15]	gPROMS® and Aspen Properties	Absorber	Rate-based mass transfer, chemical equilibrium and enhancement factor	Steady-state model validation with experimental data by Jassim et al. [6].	• Tested and compared different correlations for predicting effective interfacial area, liquid film mass transfer coefficient and gas film mass transfer coefficient. Derivation of new data for the gas film mass transfer coefficient.
Im et al. [10]	gPROMS® and Aspen Properties	Absorber	Rate-based mass transfer, chemical equilibrium and enhancement factor	Steady-state model validation with experimental data by Jassim et al. [6]	• Steady-state process optimization to minimize the total energy consumption of the RPB-based CO_2 capture process with MEA

ACM can also be packaged and exported to Aspen Plus to build and test new processes.

1.3. Novelty

Previous studies [6,8,10–12] on CO_2 absorption with MEA in RPB absorbers have reported that the size of the absorber could be significantly reduced compared to packed bed (PB) absorbers. This is because the diameter and the axial depth of the packing required by the RPB absorbers to fulfil the CO_2 separation are orders of magnitude lower than PB absorbers. For instance, Agarwal et al. [17] reported that the diameter and the axial height were reduced by 10 and 4 times when an RPB was used instead of PB for CO_2 capture. This resulted in a 7 times volume reduction factor for the RPB absorber compared to the PB absorber. Similarly, for a PCC process, Joel et al. [8] reported a 12 times reduction in volume from 0.4718 m^3 with the PB absorber to 0.04095 m^3 with the RPB absorber. Recently, Im et al. [10] reported that it would require an RPB absorber with 3 times less volume to capture the same amount (90%) of CO_2 as the PB absorber. The size (volume) reductions reported in all the studies above were based on small RPB absorber rigs with a flue gas capacity of 0.66 kg/s or less.

Furthermore, due to the presence of a centrifugal field in RPBs, higher MEA concentrations are preferred as the benchmark solvent. In some studies [18], MEA concentration of up to 100 wt% has been used. Two MEA concentrations (55 and 75 wt%) which have been widely reported in the literature [8,10,14,19] to give good results for CO_2 capture and energy consumption are used in this study. At higher MEA concentrations:

1. A rapid reaction takes place between CO_2 and MEA. This is an important quality required of solvents in RPBs due to the lower residence time of the solvent in the RPB occasioned by the smaller packing volume of the RPB.
2. The mass transfer driving potential is enhanced.
3. The solvent flow rate required to achieve 90% CO_2 capture also decreases.
4. The reboiler duty will also reduce because of the lower heat capacity, water fraction of the concentrated MEA solution and total solvent flow rate

With these benefits, the cost implications of operating an RPB-based CO_2 capture process with concentrated MEA (>30 wt%) need to be assessed. Until now, no study has been carried out on the economic assessments of the RPB-based PCC process like its PB counterpart. More so, no study has focused on quantifying the cost of CO_2 capture for an RPB absorber applied to a large-scale (250 MWe CCGT) power plant. To achieve this, a detailed scale-up of the MEA-based PCC process using an RPB absorber was carried out based on a new iterative scale-up procedure proposed in this study. This is followed by detailed technical and economic assessments to objectively quantify the costs (capital cost, operating cost, total annual cost and CO_2 capture cost) of CO_2 capture using an RPB absorber operated with concentrated (55 and 75 wt%) MEA to treat the flue gas from a 250 MW_e CCGT power plant.

1.4. RPB operating principles

An RPB is made up of a rotor (annular packed bed) fastened to two disks that are mounted on a rotating shaft. The components of the RPB are housed in a casing. Depending on the RPB design, the liquid (MEA) and the gas (Flue gas) flow across the bed in either co-current or counter-current mode. The gas flows inward radially from the outer edge of the RPB due to the pressure gradient. The liquid on the other hand is sprayed by coaxially placed liquid distributors and flows radially as thin liquid film and tiny liquid droplets from the inner radius of the packing toward the outer radius due to centrifugal acceleration. As the liquid and the gas move radially through the RPB, they are subjected to centrifugal acceleration that is many times greater than the gravitational acceleration in PBs. This enhances the mass transfer (in the packing bed and between the packing bed and the casing) and helps the separation process. This is responsible for the significant reduction in packing volume required by the RPB to fulfil a separation requirement compared to PB. The flooding limit in RPB is also extended [20,21]. Among the common materials used as a bed in the RPB is expamet [6], beads [22] and wire mesh [23]. The cross-sectional view of a typical RPB is represented in Fig. 1.

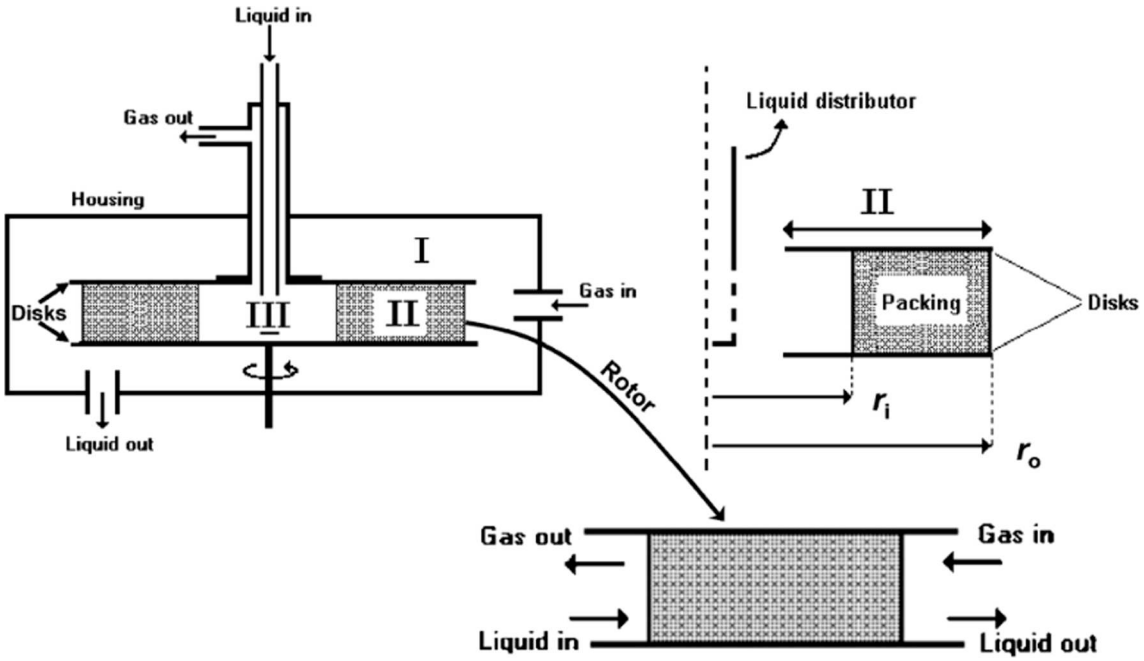

Fig. 1. Cross-sectional view of RPB [24].

2. Model development for the RPB absorber

2.1. Model assumptions

The following assumptions have been made to successfully model the RPB absorber.

- Steady-state conditions.
- The gas phase is an ideal gas.
- The vapour phase consists of CO_2, H_2O, N_2 and MEA.
- One-dimensional differential mass and energy balances for both the liquid phase and the gas phase.
- Fluid flow only in the radial direction
- All reactions occur in the liquid film and they are accounted for via the enhancement factor.
- The liquid phase consists of components such as CO_2, H_2O, N_2 MEA, OH^-, H_3O^+, HCO_3^-, CO_3^{2-}, $MEAH^+$, and $MEACOO^-$.
- Only components CO_2, H_2O, N_2 and MEA are considered in the mass transfer between the liquid and the gas phases
- No heat loss.

2.2. Material and energy balances

The material and energy balance equations are fundamental to modelling the CO_2 absorption process. For the RPB absorber, these equations are derived from the modification of the balance equations for the PB absorber. The description of all the terms in the model equations is presented in the Nomenclature section.

2.2.1. Material balance for the gas and liquid phases

Based on the model assumptions listed in Section 2.1, the material balance equations describing the mass balances for the gas phase and liquid phase in the RPB are as follows:

Gas phase:

$$0 = \frac{1}{A_c}\frac{\partial(F_l y_i)}{\partial r} - a_{gl}N_i \tag{1}$$

Liquid phase:

$$0 = -\frac{1}{A_c}\frac{\partial(F_g x_i)}{\partial r} + a_{gl}N_i \tag{2}$$

2.2.2. Energy balances for the gas and liquid phases

The equations describing the energy balance for the gas and liquid phases are as follows:

Gas phase:

$$0 = \frac{1}{A_c}\frac{\partial(F_g C_{pg} T_g)}{\partial r} - a_{gl}h_{gl}(T_l - T_g) \tag{3}$$

Liquid phase:

$$0 = -\frac{1}{A_c}\frac{\partial(F_l C_{pl} T_l)}{\partial r} + a_{gl}\left(h_{gl}(T_l - T_g) - \Delta H_{rxn_{CO_2}} N_{CO_2} - \Delta H_{vap,_{H_2O}} N_{H_2O}\right) \tag{4}$$

where $\Delta H_{rxn_{CO_2}}$ represents the heat of absorption of CO_2 with a value of 87,000 kJ/kmol [11]. The heat of vaporization of water ($\Delta H_{vap,_{H_2O}}$) is computed with the Watson's equation [25] as follows:

$$\frac{\Delta H_{vap_{H_2O,bp}}}{\Delta H_{vap,_{H_2O}}} = \left(\frac{T_c - T_{bp}}{T_c - T_l}\right)^{0.38} \tag{5}$$

where the value of T_{bp} which is the temperature of water at the boiling point is 373.15 K, and the value of T_c which is the critical temperature is 647.3 K. $\Delta H_{vap,H2O,bp}$ is the heat of vaporization at boiling point with the value of 40,660 kJ/kmol [25].

2.3. Heat and mass transfers model

The gas–liquid interfacial heat transfer coefficient (h_{gl}) in the model is determined using the Chilton-Colburn analogy [26].

$$h_{gl} = k_{lave}\rho_l C_{pl}\left(\frac{\lambda_l}{\rho_l C_{pl} D_{lave}}\right)^{\frac{2}{3}} \tag{6}$$

The rate of mass transfer of components between phases in the RPB is derived based on the two-film theory wherein the mass transfer flux is calculated as follows [11]:

$$N_i = K_{tot,i}\left(P_{gi} - P_i^*\right) \tag{7}$$

The partial pressure of component i in the gas phase (P_{g_i}) and the equilibrium partial pressure of component i (P_i^*) are calculated using a procedural call from Aspen properties®. The overall mass transfer coefficient of component i based on the gas phase ($K_{tot,i}$) is calculated from the inverse of the sum of the gas and liquid film resistances as follows.

$$K_{tot,i} = \frac{1}{\frac{RT_g}{k_{g,i}} + \frac{He_{l,i}}{E_i k_{l,i}}} \tag{8}$$

The $K_{tot,i}$ for CO_2 was calculated by considering the mass transfer resistance in the gas and the liquid films. For the other components such as N_2, H_2O, and MEA, the liquid film resistance is neglected. Thus, the $K_{tot,i}$ expression for these components becomes:

$$K_{tot,i} = \frac{k_{g,i}}{RT_g} \tag{9}$$

The enhancement factor which quantifies the effect of chemical reactions on mass transfer is calculated based on the pseudo-first-order reaction regime using the expression in Eq. (10) [5,11,27]. It depends on the concentration, rate of reaction and diffusivities of the reactants and the products.

$$E_i = \frac{\sqrt{k_{app} D_{l,CO_2}}}{k_{l,CO_2}} \tag{10}$$

The k_{app} which is the apparent reaction rate constant is determined using a termolecular kinetic model which was derived based on the overall reaction between CO_2 and MEA [28]. This termolecular kinetic model has been demonstrated to be reliable for CO_2 absorption with high MEA concentrations [5,11]. The expression for the k_{app} based on the termolecular mechanism is as follows:

$$k_{app} = 4.61x10^9 exp\left(\frac{-4412}{T}\right) Cl_{MEA}^2 + 4.55x10^6 exp\left(\frac{-3287}{T}\right) Cl_{H_2O} Cl_{MEA} \tag{11}$$

The gas film mass transfer coefficient ($k_{g,i}$) is predicted using the correlation by Chen [29] expressed in Eq. (12).

$$\frac{k_{g,i}a_{gl}}{D_g a_t^2}\left(1 - 0.9\frac{V_o}{V_t}\right) = 0.023\left(\frac{u_g\rho_g}{\mu_g a_t}\right)^{1.13}\left(\frac{u_l\rho_l}{\mu_l a_t}\right)^{0.14}\left(\frac{d_p^3\rho_g^2 r\omega^2}{\mu_g^2}\right)^{0.31}\left(\frac{u_l^2\rho_l}{a_t\sigma}\right)^{0.07}\left(\frac{a_t}{a_p}\right)^{1.4} \tag{12}$$

The correlation of Chen [29] was developed based on the two-film theory and accounted for packing geometry, end effects and centrifugal acceleration. This makes this correlation a better option for calculating the gas-film mass transfer coefficient compared to other correlations such as the Onda et al. [30] that was originally developed to predict the gas-film mass transfer coefficient in PBs.

The liquid film mass transfer coefficient ($k_{l,i}$) is predicted using the Tung and Mah [31] correlation (Eq. (13)) which has been reported to give the best predictions of the liquid film mass transfer coefficient in RPBs among the set of correlations validated against experimental data [15].

$$\frac{k_{l,i}d_p}{D_l} = 0.919\left(\frac{\mu_{l,i}}{D_{l,i}\rho_{l,i}}\right)^{\frac{1}{2}}\left(\frac{a_t}{a_{gl}}\right)^{\frac{1}{3}}\left(\frac{d_p^3\rho_l^2 r\omega^2}{\mu_l^2}\right)^{\frac{1}{6}}\left(\frac{u_l\rho_l}{\mu_l a_t}\right)^{\frac{1}{3}} \tag{13}$$

2.4. Hydrodynamic models

2.4.1. Interfacial area

The interfacial area (a_{g_l}) is obtained using the correlation of Billet and Schulte [32] presented in Eq. (14). This correlation has been shown to give a more accurate and consistent prediction of the interfacial area compared to other correlations used to predict the interfacial area in RPBs.

$$\frac{a_{gl}}{a_t} = 1.5(a_t d_h)^{-0.5}\left(\frac{\rho_l u_l d_h}{\mu_l}\right)^{-0.2}\left(\frac{\rho_l u_l^2 d_h}{\sigma_l}\right)^{0.75}\left(\frac{u_l^2}{r\omega^2 d_h}\right)^{-0.45} \tag{14}$$

2.4.2. Liquid holdup

The liquid holdup is the fraction of liquid in the void of the packing. It is not only essential for effective gas–liquid mass and heat transfers but it is also necessary to determine the rates of reactions in the liquid film. The liquid holdup in this study is predicted using the correlation developed via multiple regression of experimental data collected using a resistance measurement technique by Burns et al. [33]. The Burns et al. correlation is represented by Eq. (15).

$$\varepsilon_L = 0.039\left(\frac{g}{g_0}\right)^{-0.5}\left(\frac{u_l}{U_0}\right)^{0.6}\left(\frac{\nu_l}{\nu_o}\right)^{0.22} \tag{15}$$

The gas holdup (ε_g) is calculated by subtracting the liquid holdup from the packing porosity as follows [11]:

$$\varepsilon_g = \varepsilon - \varepsilon_L \tag{16}$$

2.4.3. Gas-phase pressure drop

The pressure drop across the RPB is calculated using the Ergun-type semi-empirical relationship developed by Llerena-Chavez and Larachi [24]. This correlation recomposed the pressure drop in the RPB through the additive aggregation of effects of the gas-slip and radial acceleration, laminar and inertial drag, and centrifugal effects.

$$\Delta P_{RPB} = \frac{150(1-\varepsilon)^2\mu_g}{d_p^2\varepsilon^3}\left(\frac{Q_g}{2\pi z}\right)In\frac{r_o}{r_i} + \frac{1.75(1-\varepsilon)\rho_l}{d_p\varepsilon^3}\left(\frac{Q_g}{2\pi z}\right)^2\left(\frac{1}{r_i}-\frac{1}{r_o}\right) + \frac{1}{2}\rho_g\omega^2\left(r_o^2-r_i^2\right) + \varepsilon\left(-0.08 - Q_g + \left(2000(RPM)^{1.22}+\omega^{1.22}\right)Q_g^2\right) \tag{17}$$

where Q_g is the volumetric flow rate of the gas, μ_g is the gas viscosity and ε is the porosity of the bed.

2.5. Thermo-physical modes

2.5.1. Vapour-Liquid equilibrium

Thermodynamic properties are key parts of the CO_2 absorption process modelling, thus determining them is essential to the model's accuracy. The thermodynamic properties are calculated using the electrolyte non-random two-liquid (eNRTL) property method in Aspen properties®. This method uses the activity coefficient model to calculate the liquid phase properties and the Redlich-Kwong equation of state (RK-EoS) to calculate the gas phase properties. Since this study considers CO_2 absorption with MEA concentrations of 55–70 wt%, the default eNRTL method in Aspen properties® (which is valid for 30 wt% MEA) was updated with parameters for higher MEA concentrations [5,34] and then embedded in the ACM® platform via the physical properties configuration feature of the ACM®. This embedded eNRTL file was then used to predict the thermodynamic properties that are used to calculate the vapour-liquid equilibrium (VLE). The VLE is computed using Eqs. (18) and (98) below.

$$P_i^* = \gamma_i x_i P_i^{vap} \tag{18}$$

$$P_i^* = H_{e,i}C_{l,i}\gamma_i \tag{19}$$

where i in Eq. (18) refers to components MEA and H_2O and i in Eq. (19) refers to components CO_2 and N_2. The term γ_i refers to the activity coefficient of component i and was calculated using the eNRTL model. The term P_i^{vap} is the vapour pressures of component i. It was calculated using the extended Antoine equation. Both were called in the model within the ACM® using a functionality known as the properties procedure call.

2.5.2. Chemical equilibrium

Chemical equilibrium determines the liquid phase speciation (i.e concentration of different species in the liquid phase). The liquid speciation is described using a simplified speciation model developed for CO_2 absorption by an aqueous solution of MEA [35]. The model eliminates the complexities and the time-consuming computations associated with other speciation models. The equilibrium chemical reactions characterising the liquid phase are depicted by reactions R_1 to R_5 below:

$2H_2O \rightleftarrows H_3O^+ + OH^-$ R_1

$CO_2 + 2H_2O \rightleftarrows H_3O^+ + HCO_3^-$ R_2

$HCO_3^- + H_2O \rightleftarrows H_3O^+ + CO_3^{2-}$ R_3

$MEAH^+ + H_2O \rightleftarrows H_3O^+ + MEA$ R_4

$MEACOO^- + H_2O \rightleftarrows MEA + HCO_3^-$ R_5

According to Gabrielsen et al. [35], the reaction of CO_2 with MEA can be approximated by a chemical equilibrium reaction (R_6) at a loading range of 0.02 mol_{CO2}/mol_{MEA} to 0.48 mol_{CO2}/mol_{MEA}.

$2MEA + CO_{2(aq)} \rightleftarrows MEAH^+ + MEACOO^-$ R_6

This means that all the absorbed CO_2 reacted with the MEA to form carbamate and that the concentration of other ionic components such as HCO_3^-, OH^- and CO_3^{2-} can be neglected. For a detailed description of the

Table 2
Physical properties and their methods of calculation.

Physical properties	Correlation	Note
Liquid Density	Rackett equation [37]	Calculated by built-in properties procedure call from Aspen properties® based on temperature, pressure and composition of the liquid-phase
Liquid Viscosity	Andrade equation with Jones Dole correction for electrolyte [38,39]	Calculated by built-in properties procedure call from Aspen properties® based on temperature, pressure and composition of the liquid phase.
Gas viscosity	Chapman-Enskog model [38]	Calculated by built-in properties procedure call from Aspen properties® based on temperature, pressure and composition of the gas phase.
Liquid-specific heat capacity	Agbonghae et al. [40]	Semi-empirical correlation developed based on concentrated MEA data.
Gas-specific heat capacity	Harun [41]	N/A
Liquid surface tension	Hakim-Steinberg-Stiel with Onsager-Samaras model [39]	Good predictions and agreement with concentrated MEA data.
Liquid diffusivity	Analogy [42]	Correlation developed based on concentrated MEA data.
Gas diffusivity	Chapman-Enskog-Wilke-Lee model [43]	Calculated by built-in properties procedure call from Aspen properties® based on temperature, pressure and composition of the gas phase.

model and the associated equations, the reader is referred to [35].

2.5.3. Physical properties calculations

Physical properties namely density, viscosity, specific heat capacity, surface tension and diffusivity of the gas phase and the liquid phase are obtained directly from Aspen properties. The correlations and the method used to calculate each of these properties in the ACM are summarised in Table 2. The built-in property procedures used to estimate some of the properties in Table 1 in ACM are Fortran subroutines available in the modeller library. The physical solubility of CO_2 in MEA is represented by Henry's law constant. This was calculated using the Ying et al. [36] correlation. The correlation is based on N_2O analogy method and was developed based on concentration MEA data.

2.6. Motor power and model implementation and solution in ACM®

2.6.1. Motor power calculation

The intensification of mass transfer that leads to a smaller equipment size for the RPB is achieved through rotation of the RPB. The amount of energy consumed to rotate the RPB absorber is accounted for using the correlation of Singh et l. [44] in Eq (20).

$$P_m = 1.2 + 0.0011\rho_L r_o^2 \omega^2 Q_l \tag{20}$$

The correlation takes into account the frictional loss and the power needed to get the inlet liquid speed up to the rotational speed at the outer radius of the RPB.

2.6.2. Model implementation and solution in ACM®

In the RPB, the gas and the liquid flow counter-currently. In this model, the gas flows from the outer periphery (outer radius, r_o) to the inner periphery (inner radius, r_i) of the RPB. The liquid on the other hand flows in the opposite direction from the inner periphery (inner radius, r_i) to the outer periphery (outer radius, r_o) of the RPB. The RPB absorber model is created by declaring a domain and its properties namely length, highest-order derivative, spacing and discretization. The domain is the space over which the model variables are distributed. It is the length from r_i to r_o of the RPB.

The RPB absorber model equations consisted of algebraic and partial differential equations that were solved by discretizing into 20 elements (21 nodes) using the first-order backward finite differences method (BFDM). Node, 0 corresponds to the location of r_i and the end node (node 20) corresponds to the location of r_o. The boundary conditions used to solve for the variables of the gas and liquid phases at each discretized point between r_i and r_o of the RPB are as follows.

Mass balance

Gas-phase: $y_i = y_0$ at $r = r_o$ and $\frac{\partial(F_g y_i)}{\partial r} = 0$ at $r = r_i$.

Liquid-phase: $x_i = x_0$ at $r = r_i$ and $\frac{\partial(F_l x_i)}{\partial r} = 0$ at $r = r_o$.

Energy balance

Gas-phase: $T_g = T_{g0}$ at $r = r_o$ and $\frac{\partial(F_g C_{pg} T_g)}{\partial r} = 0$ at $r = r_i$.

liquid phase: $T_l = T_{l0}$ at $r = r_i$ and $\frac{\partial(F_l C_{pl} T_l)}{\partial r} = 0$ at $r = r_o$.

3. Model validation

3.1. Description of RPB absorber experiment

The model presented in Section 2 is validated with experimental data collected by Jassim et al. [6] with RPB of an inner diameter of 0.156 m, outer diameter of 0.396 m and axial height of 0.025 m. This RPB absorber was located in a flameproof enclosure with adequate ventilation. The rotor of the RPB was made of stainless steel while the pipings and storage tanks were made of polypropylene. The RPB was packed with an expamet stainless steel mesh with porosity and surface area of 0.76 m^3/m^3 and 2132 m^2/m^3.

The experimental data were collected for four Cases. Each Case consisted of four experimental Runs with varying lean solvent temperatures and CO_2 loading. The CO_2 absorption was carried out using a lean solvent with average MEA concentrations of 55 wt% and 75 wt% and mass flow rates of 0.35 kg/s and 0.66 kg/s respectively. The flue gas flow rate and temperature were maintained at 2.87 kmol/h and 283.15 K throughout the experiment. The RPB was operated with a rotational speed of either 600 RPM or 1000 RPM. The details of each experimental Case and the four Runs associated with it are presented in Tables 3–6.

3.2. Model validation results

The RPB absorber model predictions of the CO_2 capture level which is described by Eq. (21) and the rich solvent CO_2 loading which is described by Eq. (22) were validated against experimental data.

$$CO_2 capturelevel(\%) = \left(\frac{y_{CO_{2,in}} - y_{CO_{2,out}}}{y_{CO_{2,in}}}\right) \times 100 \tag{21}$$

$$CO_2 loading\left(\frac{mol_{CO_2}}{mol_{MEA}}\right) = \frac{x_{CO2} + x_{CO_3^{2-}} + x_{HCO_3^-} + x_{MEACOO^-}}{x_{MEA} + x_{MEA^+} + x_{MEACOO^-}} \tag{22}$$

The model predictions are compared to the experimental data in Tables 7–10. The model generally predicted the CO_2 capture level and the rich solvent CO_2 loading to within ± 6%. A maximum relative error of 5.94% was obtained between the model predictions of CO_2 capture level and experimental data for Case 3, Run 2 where 77 wt% MEA and a rotation speed of 600 RPM were used.

Likewise, the model prediction of the rich CO_2 loadings also agree well with the experimental data. For all the Cases, the relative errors are between 0% and 3.46%. The lower relative errors obtained for the rich loading are due to the very good performance of the Gabrielsen et al. [35] model used to predict the liquid bulk concentration. The lower relative errors (generally less than 6%) obtained in this study demonstrates the accuracy and reliability of the RPB absorber model developed in this study. The icon of the RPB absorber model developed in ACM® is

Table 3
Process input conditions for Case 1 used for RPB absorber validation [6].

Case	Run	% wt MEA	Rotor speed	Pressure	Lean temp	Lean flow	Lean loading	Gas mole fraction			Liquid mole fraction		
		% wt	RPM	bar	K	kg/s	mol_{CO2}/mol_{MEA}	CO_2	H_2O	N_2	CO_2	H_2O	MEA
1	1	56	600	1.01325	312.75	0.66	0.0772	0.0471	0.1679	0.785	0.0216	0.697	0.2814
	2	53.2	600	1.01325	293.85	0.66	0.0897	0.0460	0.169	0.785	0.0234	0.7171	0.2595
	3	56	1000	1.01325	313.25	0.66	0.0772	0.0448	0.1702	0.785	0.0216	0.697	0.2814
	4	55	1000	1.01325	294.05	0.66	0.0924	0.0445	0.1705	0.785	0.0277	0.6967	0.2756

Table 4
Process input conditions for Case 2 used for RPB absorber validation [6].

Case	Run	% wt MEA	Rotor speed	Pressure	Lean temp	Lean flow	Lean loading	Gas mole fraction			Liquid mole fraction		
		% wt	RPM	bar	K	kg/s	mol_{CO2}/mol_{MEA}	CO_2	H_2O	N_2	CO_2	H_2O	MEA
2	1	55	600	1.01325	312.65	0.35	0.1000	0.0443	0.1707	0.785	0.0276	0.697	0.2754
	2	56	600	1.01325	295.45	0.35	0.0955	0.0447	0.1703	0.785	0.0274	0.689	0.2836
	3	55	1000	1.01325	312.75	0.35	0.0996	0.0435	0.1715	0.785	0.0276	0.6969	0.2755
	4	57	1000	1.01325	295.75	0.35	0.0945	0.0409	0.1741	0.785	0.0277	0.6801	0.2922

Table 5
Process input conditions for Case 3 used for RPB absorber validation [6].

Case	Run	% wt MEA	Rotor speed	Pressure	Lean temp	Lean flow	Lean loading	Gas mole fraction			Liquid mole fraction		
		% wt	RPM	bar	K	kg/s	mol_{CO2}/mol_{MEA}	CO_2	H_2O	N_2	CO_2	H_2O	MEA
3	1	75	600	1.01325	314.15	0.66	0.0492	0.044	0.171	0.785	0.024	0.4904	0.4856
	2	77	600	1.01325	294.55	0.66	0.0389	0.0436	0.1714	0.785	0.020	0.4688	0.5112
	3	74	1000	1.01325	313.35	0.66	0.0483	0.0436	0.1715	0.785	0.0229	0.5057	0.4714
	4	75.1	1000	1.01325	293.85	0.66	0.0355	0.0429	0.1721	0.785	0.0169	0.5008	0.4823

Table 6
Process input conditions for Case 4 used for RPB absorber validation [6].

Case	Run	% wt MEA	Rotor speed	Pressure	Lean temp	Lean flow	Lean loading	Gas mole fraction			Liquid mole fraction		
		% wt	RPM	bar	K	kg/s	mol_{CO2}/mol_{MEA}	CO_2	H_2O	N_2	CO_2	H_2O	MEA
4	1	72	600	1.01325	313.95	0.35	0.0582	0.0355	0.1795	0.785	0.0263	0.5262	0.4475
	2	76	600	1.01325	295.25	0.35	0.0443	0.0438	0.1712	0.785	0.0221	0.4795	0.4984
	3	75	1000	1.01325	312.55	0.35	0.0523	0.0438	0.1712	0.785	0.0256	0.4876	0.4868
	4	78	1000	1.01325	293.75	0.35	0.0407	0.0453	0.1697	0.785	0.0215	0.4515	0.527

Table 7
Model predictions versus experimental data for Case 1.

Case		1			
Run		1	2	3	4
CO2 capture level (%)	Experiment	94.9	83.0	95.4	87.0
	Model prediction	94.6	84.1	99.2	88.7
	Relative error (%)	0.32	−1.33	−3.98	−1.95
Rich loading (mol_{CO2}/mol_{MEA})	Experiment	0.0822	0.0951	0.0826	0.0955
	Model prediction	0.0823	0.0950	0.0826	0.0988
	Relative error (%)	−0.12	0.11	–	−3.46

Table 8
Model predictions versus experimental data for Case 2.

Case		2			
Run		1	2	3	4
CO2 capture level (%)	Experiment	87.0	84.1	89.9	86.2
	Model prediction	89.8	83.4	93.6	87.3
	Relative error (%)	−3.21	0.83	−4.20	−1.28
Rich loading (mol_{CO2}/mol_{MEA})	Experiment	0.1105	0.1044	0.1073	0.1021
	Model prediction	0.1100	0.1050	0.1074	0.1020
	Relative error (%)	0.45	−0.57	−0.09	0.10

presented in Fig. 2. This model icon was created using the different object shapes within ACM®.

4. Rigorous RPB design and scale-up of RPB absorber

4.1. Iterative RPB scale-up approach

Due to the paucity of data for industrial-size RPB, its design often relies on correlations to estimate its basic dimensions such as the inner radius, the outer radius, the axial height and the casing. The dimension of the RPB affects its separation performance and tendency to flood. If the height of the RPB is too small, it could result in flooding because some of the liquid will be carried away by the gas hence preventing them from reaching the inside of the RPB. On the other hand, if the height of the RPB is larger than required, parts of the packing remain unwetted by the liquid and could result in liquid maldistribution and a bulkier RPB.

Table 9
Model predictions versus experimental data for Case 3.

Case		3			
Run		1	2	3	4
CO2 capture level (%)	Experiment	98.2	84.2	97.5	91.2
	Model prediction	99.2	89.2	98.9	95.2
	Relative error (%)	−1.02	−5.94	−1.44	−4.43
Rich loading (mol_{CO2}/mol_{MEA})	Experiment	0.0531	0.042	0.0505	0.0402
	Model prediction	0.0525	0.042	0.0515	0.0408
	Relative error (%)	1.13	–	−1.98	−1.57

Table 10
Model predictions versus experimental data for Case 4.

Case		4			
Run		1	2	3	4
CO2 capture level (%)	Experiment	98.0	84.0	98.1	91.0
	Model prediction	97.6	86.1	99.7	95.7
	Relative error (%)	0.43	−2.45	−1.61	−5.16
Rich loading (mol_{CO2}/mol_{MEA})	Experiment	0.0635	0.0495	0.0586	0.0477
	Model prediction	0.0634	0.0496	0.0591	0.04896
	Relative error (%)	0.16	−0.20	−0.85	−2.64

Therefore, to estimate the dimension of the RPB, a rigorous design approach is required. Agarwal et al. [17] presented the basics of designing the RPB, thus following this procedure, a rigorous iterative scale-up approach is developed and applied to determine the dimensions of the large-scale RPB absorber in this study. The iterative approach is presented in Fig. 3. Other approaches assume K_{tot} values obtained from experimental pilot rigs. However, K_{tot} depends on the flow rate and the packing dimensions. As a result, K_{tot} values from a pilot rig will not be applicable at a large-scale plant. Additionally, the approach here adopts the area of a transfer unit (ATU) which addresses the polar coordinate issue in RPBs.

The starting point for the iterative procedure is to determine the flow rate of the lean solvent. The lean solvent mass flow rate is estimated with Eq. (23) [45] which is accurate for calculating the lean solvent flow rate in CO_2 capture with amine solvents [45–48].

$$L = \frac{Gx_{CO2}\Psi_{CO2}}{100\tilde{z}(\Delta\alpha)}\left[\frac{M_{MEA}}{44.009}\left(1+\frac{1-\omega_{MEA}}{\omega_{MEA}}\right)+z\alpha_{lean}\right] \tag{23}$$

The inner radius (r_i) of the RPB is estimated from Eq. (24) [17]. The inner radius houses the liquid distributor and therefore it must be designed in such a way that will not lead to high exit gas velocity that could break the liquid jets from the liquid distributor. Moreover, it must allow for gas withdrawal from the RPB without causing an excessive pressure drop.

$$r_i = \left(\frac{Q_G}{\pi U_{jet}(1-f_d)}\right)^{1/2}\left(\frac{\rho_g p^{l/g}}{\rho_l}\right)^{1/4} \tag{24}$$

The axial height (Z) of the RPB is calculated based on the superficial velocity of the gas at flooding. An excessive splashing of the MEA solvent in the rotor eye occurs at flooding [6], thus the RPB must be designed to operate below flooding. The superficial velocity of the gas at flooding is calculated using the expression in Eq. (25) which is a unique correlation developed by Jassim et al. [6] for RPB with expamet packing based on the functional form of the Sherwood plot.

$$\mathrm{In}\left[\frac{U_{g,fl}^2 a_t}{r_i\omega^2\varepsilon^3}\left(\frac{\rho_g}{\rho_l}\right)\right] = -3.01-1.40In\left(\frac{L}{G}\sqrt{\frac{\rho_g}{\rho_l}}\right)-0.15\left[\mathrm{In}\left(\frac{L}{G}\sqrt{\frac{\rho_g}{\rho_l}}\right)\right]^2 \tag{25}$$

Because of their higher flooding capability, RPBs can be designed to operate at about 80% flooding [49,50], thus the operating superficial gas velocity (U_g) and the axial height of the RPB are computed from Eqs. (26) and (27) respectively.

$$U_g = f\ U_{g\text{-}fl} \tag{26}$$

$$Z = \frac{Q_g}{2\pi r_i U_g} \tag{27}$$

The outer radius (r_o) of the RPB is calculated iteratively. Firstly, a value is assumed for the outer radius. Then the value of $K_{\_tot}$ and the effective interfacial area (a_t) was determined as shown in Fig. 3. Following this, the area of a transfer unit (ATU) and the number of transfer units (NTU) are obtained as follows:

$$ATU = \frac{F_g}{ZK_{tot}P} \tag{28}$$

$$NTU = \int_{y_1}^{y_2}\frac{dy}{y-y_e} \tag{29}$$

Assuming a negligible value of y_e, then Eq. (29) reduces to.

$$NTU = In\frac{y_2}{y_1} \tag{30}$$

Then, finally, the outer radius of the RPB is calculated using Eq. (31) and Eq. (32).

$$\pi\left(r_o^2 - r_i^2\right) = ATU \times NTU \tag{31}$$

$$r_o^2 = \frac{ATU \times NTU}{\pi} + r_i^2 \tag{32}$$

4.2. RPB absorber for large-scale PCC plant

The scale-up procedure described in Section 4.1 is applied to design a large-scale RPB absorber based on MEA solvent to capture CO_2 from a 250 CCGT power plant. The condition of the flue gas from the CCGT power plant is listed in Table 11. This flue gas condition corresponds to those obtained after pre-treatment to remove contaminants such as particulates, SO_2 and NO_x [51].

The flow rate of the MEA solvent required to capture 90% of CO_2 in the flue gas is calculated from Eq. (23). based on an absorption capacity of 0.18 mol_{CO2} /mol_{MEA}. This absorption capacity is a conservative value. Below 0.18 mol_{CO2} /mol_{MEA}, the estimated solvent flows become so large that if adopted, the size-reduction expectation of the RPB absorber may not be met. The presence of centrifugal acceleration in the RPB could lead to higher CO_2 uptake which may result in a higher value of absorption capacity.

The results in Table 12, show that the concentration of the MEA is very influential on the amount of solvent required for CO_2 capture. As the concentration of the MEA increases from 55 wt% to 75 wt%, the lean solvent flow rate reduced from 368.48 kg/s to 277.44 kg/s and the L/G ratio reduced by 75% from 1.04 kg/kg to 0.78 kg/kg. These solvent flow rates and the flue gas flow rate were used to estimate the dimensions of the large-scale RPB absorber.

The inner radius of the RPB is calculated with Eq. (24). The recommended liquid jet velocity (U_{jet}) of 4.5 m/s is adopted [17]. The values of ρ_G and ρ_l are estimated from Aspen Properties at temperature of 313.14 K, pressure of 1.01 bar and lean loading of 0.2 mol_{CO2}/mol_{MEA}. The results in Table 12 show that r_i only slightly reduced (by about 0.7%)

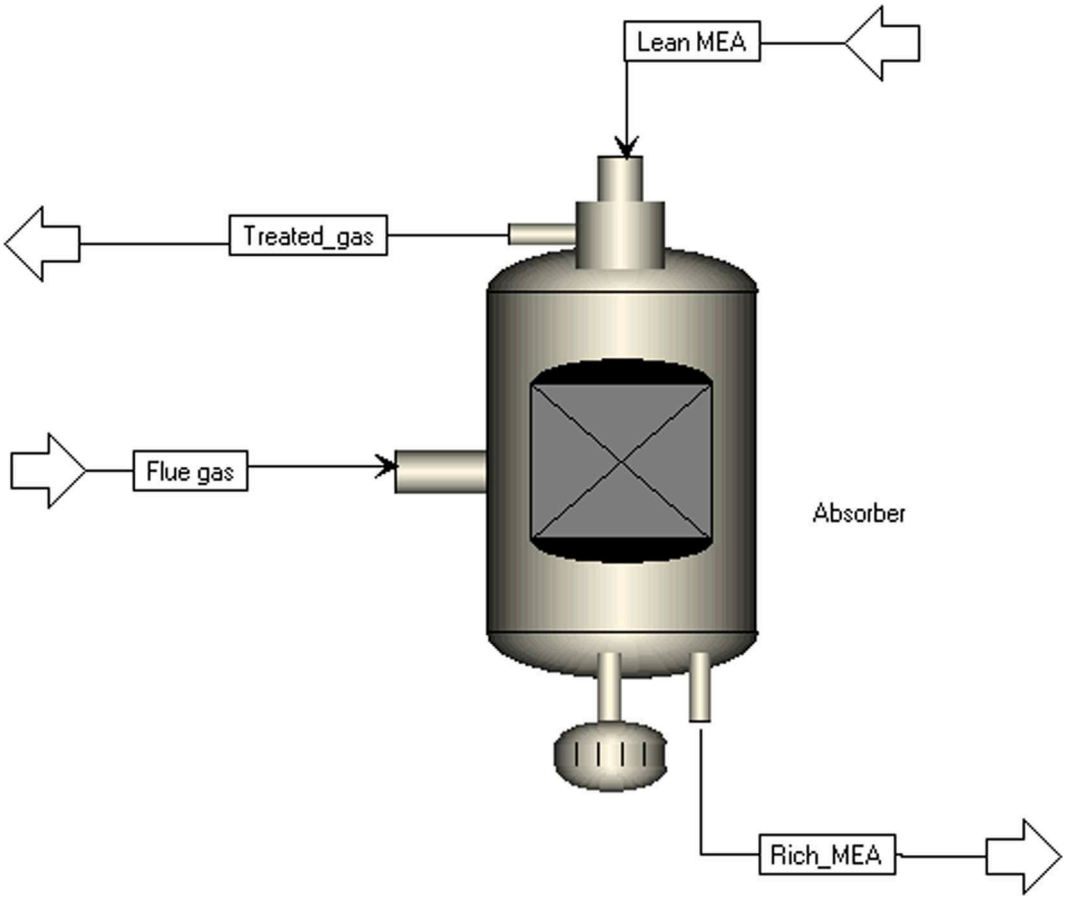

Fig. 2. Icon of the RPB absorber model developed in ACM®.

despite a 36% increase in MEA concentration. The reason for this small change in r_i is that all the terms in the equation (Eq. (24)) used to calculate r_i are constant except for ρ_l which changed from 1062.64 kg/m^3 at 55 wt% MEA concentration to 1084.38 kg/m^3 at 75 wt% MEA concentration.

The results for the axial height of the RPB (Table 12) indicate that the change in MEA concentration from 55 wt% to 75 wt% has a more profound effect on the axial height of the RPB than on r_i. The axial height decreased by about 6% which is about 5.3% more than the size reduction achieved in r_i. The outer radius (r_o) of the RPB also reduced as the MEA concentration increased from 55 wt% to 75 wt% (see Table 12). This reduction in r_o is because of the reduction in ATU and r_i of the RPB. The reduction in the ATU is influenced by K_{tot} and the axial height of the RPB.

So far, studies on the application of RPB for CO_2 capture are limited to the pilot scale. Thus, data on the maximum allowable outer diameter for a large-scale RPB is not available in the literature. However, it was recommended that the ratio Z/r_o should not exceed the limit of 0.85 for RPB design [49]. This ratio is 0.26 for the RPB designed in this study. A conservative maximum diameter of 10 m was used to design the large-scale RPB absorber in this study. This was chosen because of the limitation imposed by the moving mechanical parts of the RPB. For packed columns with no moving parts, the recommended maximum diameter could be as high as 18 m [45,46,52].

5. Technical and economic assessments of the large-scale MEA-based RPB absorber

5.1. Technical assessment

Process analysis of CO_2 capture with MEA in pilot-scale RPB absorbers has been carried out [6,8,11,14] to investigate the influence of important process variables on its performance. Findings from these studies have confirmed the size-reduction capability of the RPB. However, these analyses were performed using small RPB rigs and process conditions (lean loadings (0.0355–0.10 mol_{CO2}/mol_{MEA}), rich loadings (0.0420–0.111 mol_{CO2}/mol_{MEA}), lean temperature (20 °C) and the L/G ratio (16–30 kg/kg)) that are economically impractical for the CO_2 capture process. The process analysis performed in this study employs practicable conditions to technically assessed the performance of the large-scale MEA-based RPB absorber. The operating conditions and the specifications presented in Table 12 are used to simulate the large-scale RPB absorber.

5.1.1. Lean solvent CO_2 loading

The amount of CO_2 in the lean solvent affects the capture level and rich loading in the RPB absorber. The impact of the lean loading on the capture level is investigated by varying the lean loading from 0.16 to 0.3 mol_{CO2}/mol_{MEA} at MEA concentrations of 55 and 75 wt%. The rotor speed is maintained at 600 RPM for this analysis. Results in Fig. 4 indicate that the CO_2 capture level decreases as the lean loading increases for both MEA concentrations. The decrease is however more profound for 55 wt% MEA than for 75 wt% MEA. This is because the absorption capacity of the 55 wt% MEA reduces faster as the lean loading increases. This results in lesser free MEA available to react with CO_2 at 55 wt% MEA compared to 75 wt% MEA concentration. Consequently, there is more CO_2 uptake with 75 wt% MEA at all lean loadings.

The CO_2 capture levels are below 90% at lean loadings below 0.22 mol_{CO2}/mol_{MEA} for the 55 wt% MEA. Operating at these lean loadings translates to higher regeneration to strip the lean solvent. Above 0.27 mol_{CO2}/mol_{MEA}, the capture levels drop below 90%, particularly for the 55 wt% MEA. This means that either a higher solvent rate or a higher

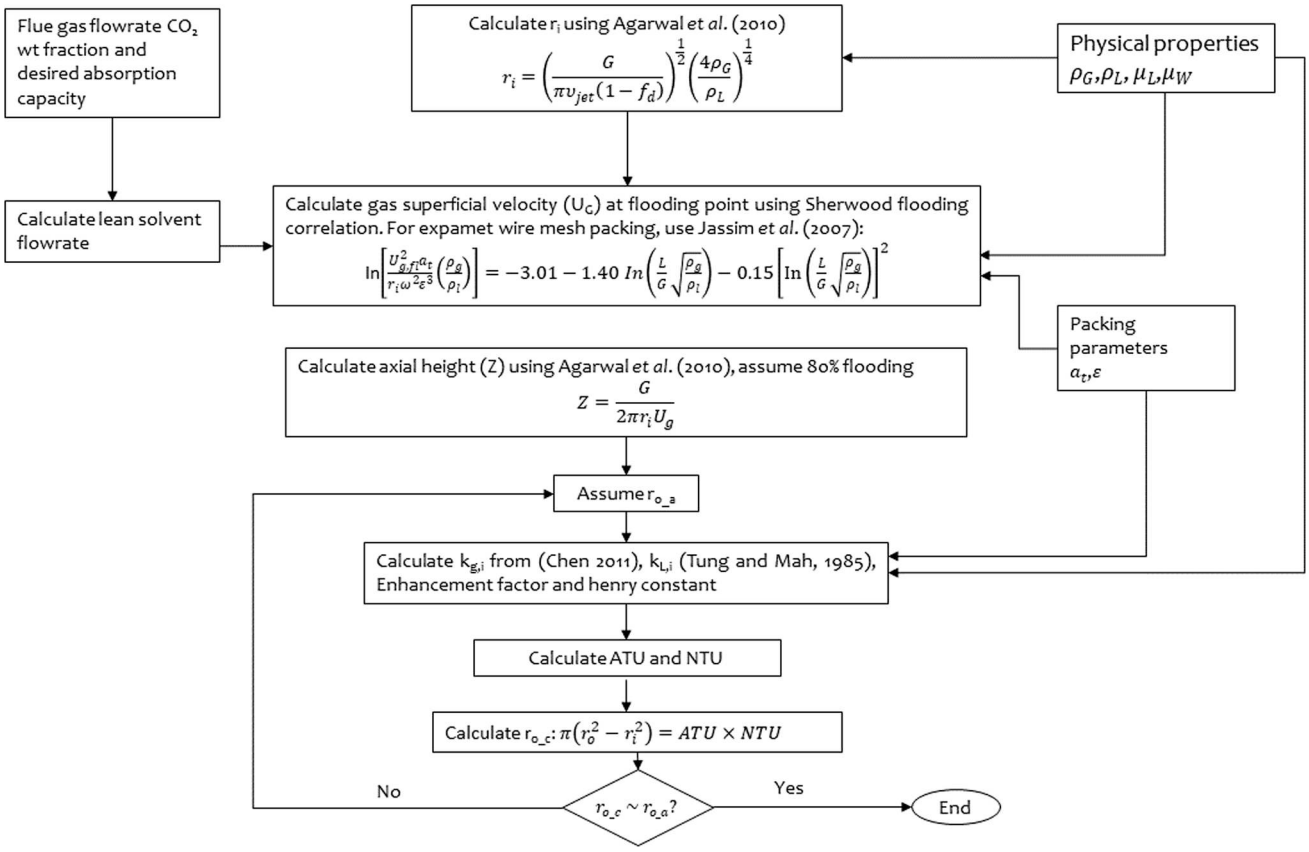

Fig. 3. Rigorous iterative scale-up approach for RPB.

Table 11
Flue gas conditions from 250 MW_e CCGT power plant [51].

Flue gas	
Flow rate (kg/h)	1,281,600
Temperature (K)	313.15
Pressure (bar)	1.01325
Components (Mole fraction)	
CO_2	0.04923
H_2O	0.08503
N2	0.86574

Table 12
Estimated dimensions and operating conditions for the large-scale RPB absorber.

	MEA concentrations	
	55	75
r_i (m)	1.48	1.47
r_o (m)	4.86	4.61
Z (m)	1.26	1.19
Lean flow rate (kg/s)	368.48	277.44
L/G ratio (kg/kg)	1.04	0.78
Lean Temperature (K)	313.15	313.15
Lean loading (mol_{CO2}/mol_{MEA})	0.16–0.30	
RPB Pressure (bar)	1.01325	
ω(rad/s)	20.94–125.65	

axial packing height will be required to attain a 90% capture level. This could increase both the capital and the operating cost of the RPB process. Thus, 0.25 mol_{CO2}/mol_{MEA} is used as the lean loading in the other analysis in this work.

The effects of lean loadings on the rich loadings are presented in Fig. 5. The rich loading increases with lean loadings as MEA concentration increases from 55 wt% to 75 wt%. This increase in rich loading is not an indication of better absorption performance. Rather it is the difference between the rich and lean loadings (absorption capacity) that does. At lower lean loadings the absorption capacities are higher than at high lean loadings. Hence higher capture levels are achieved at low lean loadings.

5.1.2. Rotor speed

Previous studies have investigated the effects of rotor speed on capture level at pilot-scale RPB absorbers. These studies found that the rotor speed enhances both mass and heat transfer which ultimately improves the absorption performance in the RPB absorber. The impacts of the rotor speed on capture level are examined at rotor speeds of 200 to 1200 RPM for both 55 wt% and 75 wt% MEA.

From the results in Fig. 6, there is a sharp increase in the capture level for both MEA concentrations up to 600 RPM. This increase in capture level plateaued at 800 RPM and remain almost the same till 1200 RPM. The reason for this is that the influence of the rotor speed on the interfacial area available for mass transfer is more significant at lower rotor speeds (200–600 RPMs) than at higher rotor speeds (800–1200 RPMs). For example, with 55 wt% MEA, the interfacial area increased by 6% from 1361.4 m^2/m^3 to 1446.95 m^2/m^3 upon increasing the rotor speed from 400 RPM to 600 RPM. This was reduced to 1.3%, 0.99% and 0.82% upon increasing the rotor speed to 800, 1000 and 1200 RPMs respectively. This indicates that it is less economical to operate the RPB absorber at rotor speed above 600 RPM as it means more rotating energy would be consumed with very few changes in capture level.

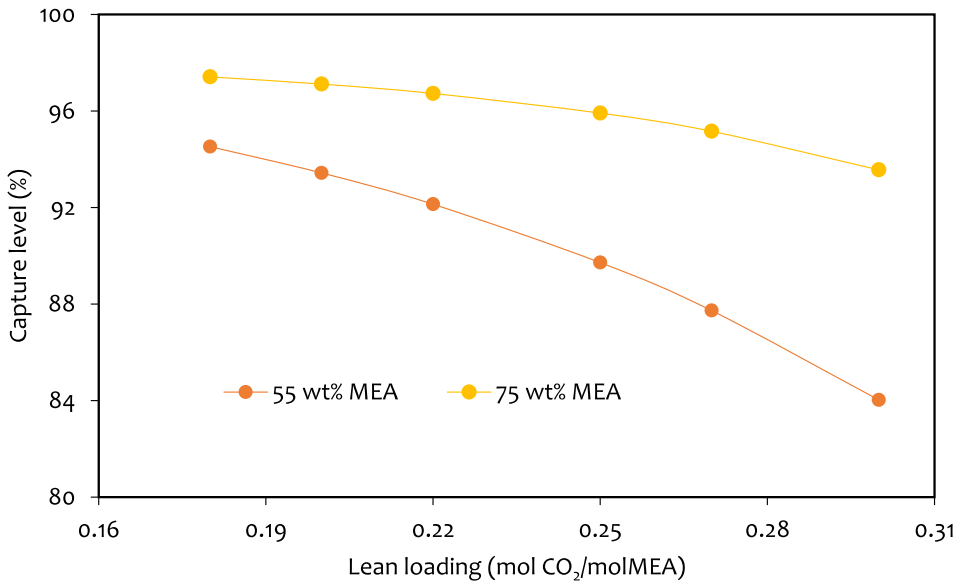

Fig. 4. Effects of lean loading on capture level at 55 and 75 wt% MEA concentrations.

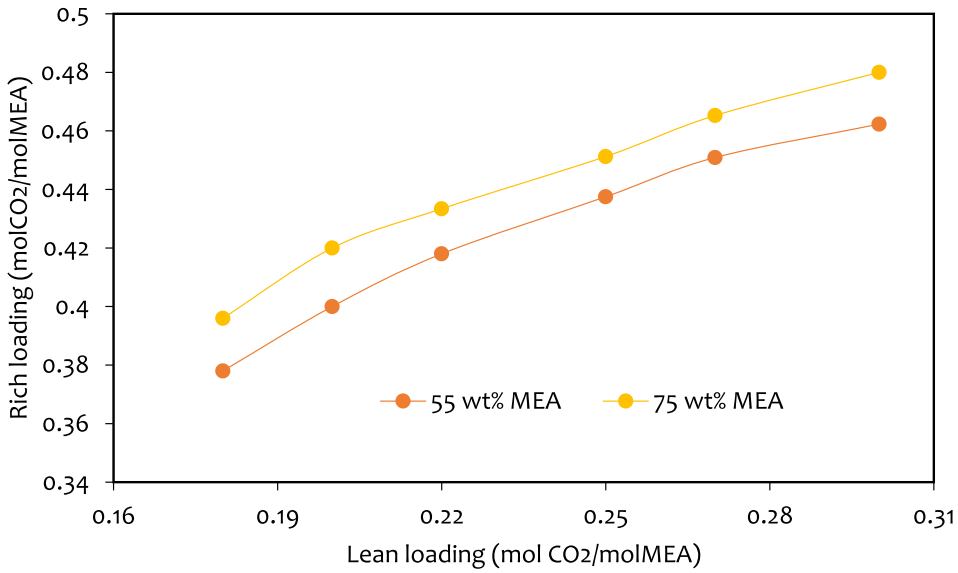

Fig. 5. Effects of lean loading on rich loading at 55 and 75 wt% MEA concentrations.

5.1.3. Lean MEA flow rate

This analysis is carried out by varying the lean MEA flow rate from 260 to 440 kg/s. The rotor speed is maintained at 200 RPM. As mentioned earlier, in the pilot-plant experiments by Jassim et al. [6] and subsequent studies by other researchers, L/G ratios of 16–30 were used. These L/G ratios could lead to flooding issues, higher energy for solvent regeneration and an RPB with a large inner diameter and height. The L/G ratio should be kept low to avoid these issues [10] thus these solvent flows resulted in L/G ratios of between 0.73 kg/kg and 1.24 kg/kg for this study.

Fig. 7 shows the results of the effects of lean MEA flow rate variation on the capture level The capture level increases as the lean MEA flow increases for both MEA concentrations. This means as the solvent flow increases, more MEA is available to react with the CO_2 in the flue gas thereby leading to a higher capture level. Higher capture levels are achieved at 75 wt% MEA concentration. The capture levels are generally below 90% at 55 wt% MEA. On increasing concentration to 75 wt%, the capture levels get to above 90%. In previous studies [8,14], the capture levels at these conditions are usually close to 100% because of the excessive L/G ratio used. The lean MEA flow rates used in this study resulted in realistic and practicable L/G ratios.

5.1.4. Motor energy consumption

Additional parasitic energy is incurred to rotate the RPB absorber. This with the regeneration energy could result in higher total energy consumption for the RPB absorber. The rotor power consumptions are estimated at 200–1000 RPMs for both 54 wt% MEA and 75 wt% MEA. Fig. 8 shows how the power consumption varied with rotor speeds at two MEA concentrations. Generally, the rotor power consumption increases with rotor speed for both MEA concentrations. Expectedly, the power consumptions are higher for the 55 wt% MEA compared to 75% MEA. This is because Eq. (20) used to calculate the motor power consumption is based on the solvent volumetric flow rate (Q_l), outer radius (r_o), rotational speed (ω) and liquid density (ρ_L). The values of the Q_l and r_o are particularly lower at 75 wt% MEA than at 55 wt% MEA. Generally, these results suggest that it is more economical to operate the RPB

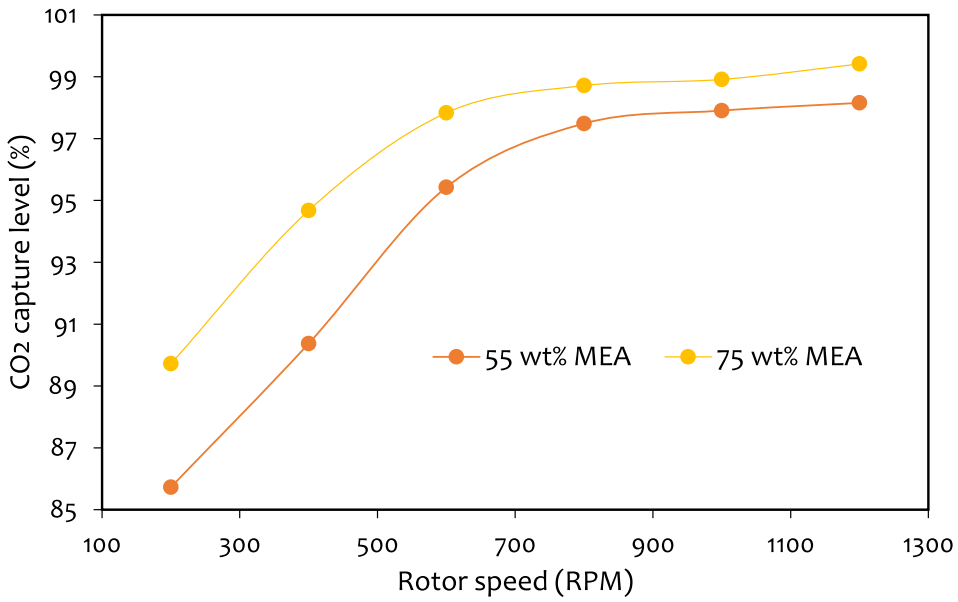

Fig. 6. Effects of rotor speed on capture level at 55 and 75 wt% MEA concentrations.

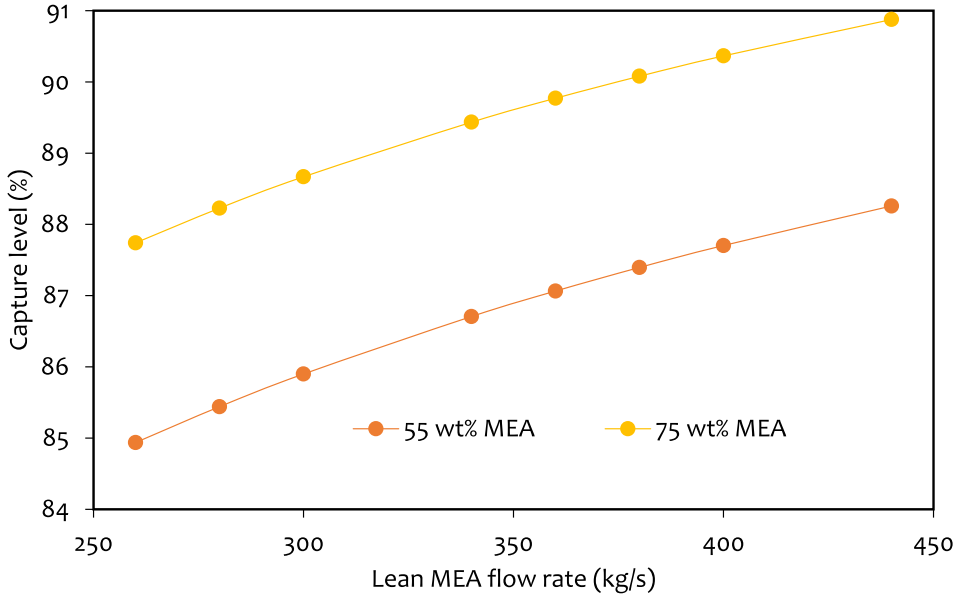

Fig. 7. Effects of lean MEA solvent flow rate on capture level at 55 and 75 wt% MEA concentrations.

absorber at rotor speeds of 600 RPM and below.

5.2. Economic assessments of the large-scale MEA-based RPB absorber

So far, no study has reported on the cost of CO_2 capture in RPBs. In this study, the economic assessments are performed to estimate the capital expenditure (CAPEX), the operating cost (OPC), the total annual cost (TAC) and the CO_2 capture cost of a large-scale MEA-based RPB absorber operated with 55 wt% and 75 wt% MEA concentrations. The economic assessments are carried out at 200 RPM using the specifications in Table 11.

Since there are no industrial experiences or established and detailed cost data for the costing of RPBs (particularly for CO_2 capture applications), calculating the CAPEX, the OPEX, as well as other costs relating to RPBs, relies heavily on cost correlations. These correlations have been applied to the costing of RPBs used in distillation [50], recovery and purification of bioethanol [49] and aroma absorption from bioreactor off-gas [53]. The general costing procedures adopted in this study followed the ones provided in these studies. The CAPEX of the RPB is calculated from Eq. (33) based on the annual amortization of the total capital cost (TCC).

$$CAPEX_{RPB} = TCC \times amortizationfactor \tag{33}$$

The amortization factor which is the addition of annual capital depreciation (10%), interest rate (10%), profit margin (10%) and maintenance (3%) is set to 0.33 [53]. The TCC is the product of the equipment purchase cost (EPC) of RPB and the Lang factors (F_{lang}). The F_{lang} has a value of 4.7 and represents the costs (direct and indirect) and fees associated with the plant set-up [53].

$$TCC = EPC \times F_{lang} \tag{34}$$

The EPC is made up of three parts namely (I) costs for the motor (C^{motor}), (II) the costs for the rotor (C^{rotor}) which also include the cost of packings, shafts, liquid distributors and casing, and (III) the costs for the

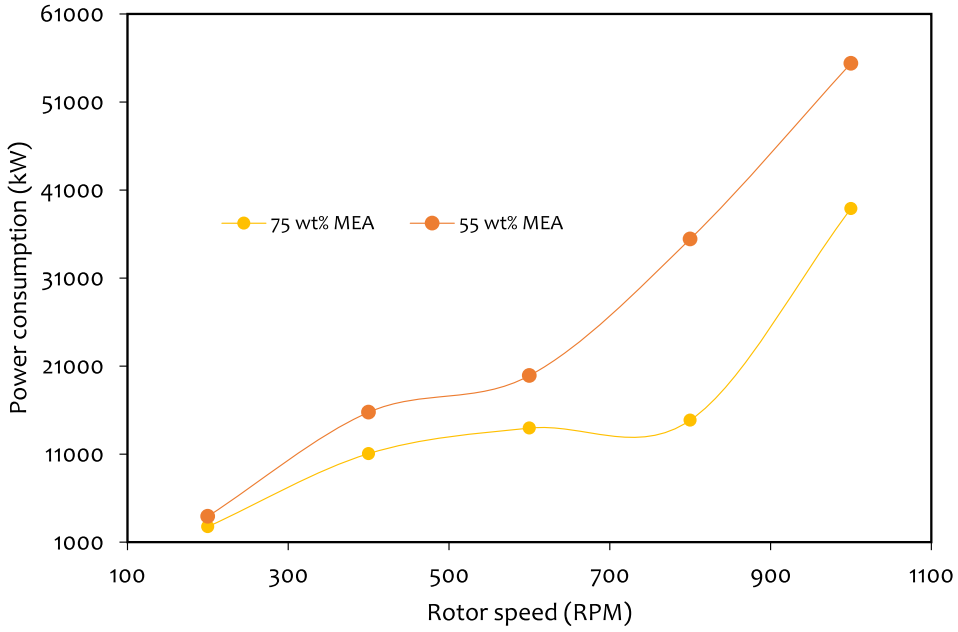

Fig. 8. Power consumption at different rotor speeds and MEA concentrations of 55 and 75 wt%.

drives, rotating parts and bearings (C^{drive}) [50]. C^{tax} is the added tax on the cost of materials.

$$EPC_{RPB} = \left(C^{rotor} + C^{motor} + C^{drive}\right) \times C^{tax} \quad (35)$$

The cost of each part of Eq. (35) is calculated with the expression in Eq. (36).

$$C^{i} = {C_{FOB}}^{i}\left(1 + C^{i}_{L+M}C^{i}_{L/M}\right) \times \frac{C^{CEPCI}}{1000} \quad (36)$$

Where i is for rotor, motor or drive and ${C_{FOB}}^{i}$ is the free-on-board (FOB) cost of materials and construction. It is computed with Eqs. (37)–(39).

$${C_{FOB}}^{rotor} = {C_{ref}}^{rotor} \times \left(\frac{V^{RPB}}{{V_{ref}}^{RPB}}\right)^{n^{rotor}} \quad (37)$$

$${C_{FOB}}^{motor} = {C_{ref}}^{motor} \times \left(\frac{P^{motor}}{{P_{ref}}^{motor}}\right)^{n^{motor}} \times C^{RS} \times C^{en} \times C^{al} \quad (38)$$

$${C_{FOB}}^{drive} = {C_{ref}}^{drive} \times \left(\frac{P^{motor} \times {C_{trans}}^{0.5}}{{P_{ref}}^{drive}}\right)^{n^{drive}} C^{al} \quad (39)$$

The descriptions of the terms in Eqs. (35)–(39) are provided in the nomenclature and their respective values and detailed descriptions are available in [50].

Table 13
FOB and CAPEX for the large-scale RPB absorber for solvent-based PCC.

Cost	Value (M$)	
	55 wt% MEA	75 wt% MEA
${C_{FOB}}^{rotor}$ (M$)	1.52	1.37
${C_{FOB}}^{motor}$ (M$)	0.91	0.91
${C_{FOB}}^{drive}$ (M$)	4.42	4.42
C^{rotor} (M$)	2.39	2.16
C^{motor} (M$)	0.95	0.95
C^{drive} (M$)	3.40	3.36
C^{tax}	1.19	1.19
EPC (M$)	7.98	7.70
TCC (M$)	37.5	36.2
$CAPEX_{RPB}$ (M$)	12.30	11.90

The OPC of the RPB absorber (OPC_{RPB}) was estimated as the sum of the fixed operating cost (FOC) and the variable operating cost (VOC). The FOC was estimated to be 4% of the $CAPEX_{RPB}$ [48] and the VOC was estimated using Eq. (40). It is the product of the electrical power consumed by the motor (P_m), cost of electricity (C_{elec} = 0.144/kWh) and operating time per year (t_{yr} = 8000 h/yr) [49,53].

$$VOC = P_m C_{elec} t_{yr} \quad (40)$$

The annualized CAPEX was calculated by dividing the CAPEX by the capital recovery factor (CRF). The CRF was estimated from Eq. (41).

$$CRF = \frac{(1+i)^n - 1}{i(1+i)^n} \quad (41)$$

where n is the project life of 20 years and i is the interest rate of 10%. The total annual cost of the RPB (TAC_{RPB}) is the sum of the annualized CAPEX and the OPC_{RPB} (Eq. (41)).

$$TAC_{RPB} = annualizedCAPEX_{RPB} + OPC_{RPB} \quad (42)$$

The cost of CO_2 captured was estimated by dividing the TAC by the total amount of CO_2 captured per year. The estimated CAPEX is shown in Table 13. The results of the annualized CAPEX, OPC and the TAC of the large-scale RPB absorber are presented in Table 15.

Table 14
Comparison of the size of RPB and PB absorbers for CO_2 capture from a 250 MW_e CCGT power plant.

Configurations	PB absorbers			RPB absorbers	
	Standard	Standard	Al	RPB	RPB
Solvent	MEA	PZ	PZ	MEA	MEA
Solvent conc (wt%)	30	40	40	55	75
Inner diameter (m)				2.96	2.94
Outer diameter (m)	14	12.5	12	9.72	9.22
packing height (m)	30	20	15	1.26	1.19
Packing volume (m^3)	4618	2454	1697	94	80
Packing volume reduction (times)				18–49	21–58
Unit volume (m^3)	4618[a]	2454[a]	1697[a]	423[b]	360[b]
Volume reduction (times)				4–11	5–13

[a] Without the sump [b]calculated based on the assumptions provided in [17].

5.3. Comparison between large-scale CO_2 capture based on PB and RPB

5.3.1. Size

The size of the large-scale MEA-based RPB absorber is compared to that of PB absorbers reported by Otitoju et al. [48]. The PB absorbers were designed for CO_2 capture with 30 wt% MEA and 40 wt% PZ from a 250 MW_e CCGT power plant. The same flue gas conditions used in this study were also used in that study. Two absorber configurations namely a Standard absorber and an absorber with intercooling (AI) were designed. The standard absorber was operated with both 30 wt% MEA and 40 wt% PZ. The absorber with intercooling was operated with 40 wt % PZ only. The size (diameter, packing height and packing volume) of the RPB and PB absorbers are compared in Table 14 for different solvent types and concentrations. The diameter and packing height of the RPB absorber reduced significantly compared to those of the PBs. The packing volume of the RPB absorber was reduced by 18–49 times with 55 wt% MEA compared to PB absorbers. Higher packing volume reductions of 21–58 times were achieved with an RPB absorber operated with 75 wt% MEA. A 42-times reduction in packing volume (0.035 m^3 for PB vs 0.0000833 m^3 for RPB) was reported for an RPB absorber used for CO_2 absorption from the flue gas of a coal-fired power plant [54].

Furthermore, the volume of each of the PB units and the RPB unit was determined using the approach of Agarwal et al [17]. Compared to the PB absorbers, the RPB absorber operated with 55 wt% MEA has a 4–11 times volume reduction factor while that operated with 75 wt% MEA has a 5–13 times volume reduction factor. These reduction factors are consistent with that obtained for CO_2 absorption with an aqueous solution of diethanolamine (DEA) in RPB [17]. The reductions are possible because of the high centrifugal acceleration present in RPB. Since the reduction of the process equipment footprint (particularly the absorber and stripper) is one of the most relevant parameters in the CO_2 capture process, this could be achieved with the RPB technology. This technology could also be useful in space-limited applications like offshore, ships and mobile skid plants. In addition to this, RPB is capable of fulfilling larger flue gas treatment compared to PB of similar size because the gas retention time in RPB can be controlled below 1.5 s due to mass transfer intensification [54]. The gas retention time in the PB is about 20.4 s. Furthermore, the RPB technology could also reduce the cost of the process.

5.3.2. Cost

The costs of the large-scale RPB absorber are also compared to the cost of large-scale PB absorbers from Otitoju et al. [48]. In that study, the CAPEX of the standard absorbers using 30 wt% MEA and 40 wt% PZ were calculated as $25.20 million and $14.70 million while the CAPEX for the Al absorber using 40 wt% PZ was determined to be $12.63 million. With RPB absorber operated with 55 and 75 wt% MEA, the CAPEX reduced to $12.3 million and $11.9 million respectively. With 55 wt% MEA, the CAPEX of the RPB is 3–51% less than that of the PBs. Higher CAPEX reductions of 6–53% are achieved with the 75 wt% MEA.

The OPC of the PB absorbers is higher compared to the RPB absorber (Table 15). The higher OPC in the PB absorbers is due to the higher cost of solvent and water make-ups which constitutes the bulk of the OPC in the PB absorbers. The OPC for the RPB absorber mainly comes from the energy consumed to rotate the absorber. The OPC was 41–56% lower with RPB operated with 55 wt% MEA compared to the PB absorbers. Higher reductions in OPC of between 61 and 70% were attained when the RPB was used with 75 wt% MEA. These reductions in the OPC of the RPB are due mainly to the lower solvent cost resulting from a lower solvent flow rate (277 kg/s with 75 wt% MEA and 368 kg/s with 55 wt% MEA) for RPB compared to the PB absorbers (705 kg/s with 30 wt% MEA and 406 kg/s with 40 wt% PZ). The lower solvent flow rates in the RPB absorber were partly due to the intensification of the mass transfer process by the centrifugal acceleration present in the RPB absorber. In addition to this, the lower cost of the MEA solvent ($1500/tonne compared to $8000/tonne PZ [48]) also contributed to the reduction in the OPC of the RPB absorber.

Table 15
Comparison of the cost of the RPB and PB absorbers for CO_2 capture from a 250 MW_e CCGT power plant.

Configurations	PB absorbers			RPB absorbers	
	Standard	Standard	Al	RPB	RPB
Solvent	MEA	PZ	PZ	MEA	MEA
Solvent conc. (wt%)	30	40	40	55	75
Annualized CAPEX (M$/yr)	7.46	4.34	3.81	1.45	1.39
FOC (M$/yr)	2.54	1.48	1.29	0.49	0.48
VOC (M$/yr)	7.95	6.58	6.61	4.18	2.64
OPC (M$/yr)	10.49	8.06	7.90	4.67	3.12
TAC (M$/yr)	17.95	12.40	11.71	6.12	4.5
CO_2 capture cost ($/$t_{CO2}$)	24.51	16.04	15.15	9.01	6.49

As shown in Table 15, for both PB and RPB absorbers, the OPC made the largest contribution to the TAC. The OPC contributed about 58–67% to the TAC for PB absorbers and 69–76% to the TAC for RPB absorbers. The remainder of the contributions to the TAC is from the annualized CAPEX. Results for the CO_2 capture cost (Table 15) indicate that whereas it would require between $15 and 24 to capture 1 tonne of CO_2 in PB absorbers, it will require between $6.5 and $9 to capture 1 tonne of CO_2 in the RPB absorber. This represents a 42–73% reduction in CO_2 capture cost thus demonstrating the cost reduction capability of the RPB absorber.

The potential for a reduction in the CO_2 capture cost could be higher if the RPB is applied to a coal-fired power plant where the CO_2 concentration in the flue gas (12–14 mol%) could be >3 times (4–5 mol%) that of the CCGT power plant.

6. Conclusion

In this study, a steady-state rate-based model of an RPB absorber is developed in Aspen Custom Modeller®. Relevant thermodynamic and physical properties and correlations for mass transfer, chemical reactions, heat transfer coefficient and hydrodynamics were incorporated into the model. The model was validated with pilot rig data and closely predicted the pilot data with a maximum deviation of ±6%.

Following this, a new iterative scale-up procedure was proposed and used to scale up the RPB absorber to capture CO_2 from the flue gas of a 250 MW_e CCGT power plant. Technical assessments including the influence of lean loading, rotor speed and lean MEA flow rate on the performance of the RPB absorber were performed with MEA concentrations of 55 and 75 wt%. Further technical assessments showed that the size of the large-scale RPB absorbers was lower compared to PB absorbers. The RPB absorber achieved a 4–11 times and a 5–13 times volume reduction factor with 55 and 74 wt% MEA respectively. Economic assessments showed that the CAPEX of the RPB absorber is lower by 3–53%. Additionally, a CO_2 capture cost of 6.5/t_{CO2}–$9/$t_{CO2}$ was achieved with the RPB absorber compared to $15/$t_{CO2}$–$24/t_{CO2} achieved with the PB absorbers.

An integrated model of the large-scale intensified PCC process consisting of the RPB absorber, RPB stripper, heat exchangers, pumps and cooler is critical to gaining insights into the design and operations of the large-scale intensified PCC process. Also, a detailed economic assessment of the whole process is required to determine the CO_2 capture cost for the entire intensified PCC process. Furthermore, optimization of the whole process would show how the performance of the intensified PCC process could be improved.

CRediT authorship contribution statement

Olajide Otitoju: Conceptualization, Methodology, Software, Validation, Funding acquisition, Writing – original draft, Writing – review & editing. **Eni Oko:** Conceptualization, Supervision, Writing – review & editing. **Meihong Wang:** Conceptualization, Supervision, Funding

acquisition, Writing – review & editing.

Declaration of Competing Interest

The authors declare that they have no known competing financial interests or personal relationships that could have appeared to influence the work reported in this paper.

Data availability

Data will be made available on request.

Acknowledgement

The first author is grateful to the Petroleum Technology Development Fund (PTDF), Nigeria (Ref: PTDF/ED/PHD/OOS/1086/17) for providing financial support to this study. All the authors would like to acknowledge the financial support of the EU RISE project OPTIMAL (Ref 101007963).

References

[1] Aydin G, Jang H, Topal E. Energy consumption modelling using artificial neural networks: The case of the world's highest consumers. Energy Sources, Part B Econ Plan Policy 2016;11:212–9.
[2] Hong WY. A techno-economic review on carbon capture, utilisation and storage systems for achieving a net-zero CO_2 emissions future. Carbon Capture Sci Technol 2022;3:100044.
[3] Wang M, Lawal A, Stephenson P, Sidders J, Ramshaw C. Post-combustion CO_2 capture with chemical absorption: a state-of-the-art review. Chem Eng Res Des 2011;89:1609–24.
[4] Lawal A, Wang M, Stephenson P, Obi O. Demonstrating full-scale post-combustion CO_2 capture for coal-fired power plants through dynamic modelling and simulation. Fuel 2012;101:115–28.
[5] Oko E, Ramshaw C, Wang M. Study of intercooling for rotating packed bed absorbers in intensified solvent-based CO_2 capture process. Appl Energy 2018;223:302–16.
[6] Jassim MS, Rochelle G, Eimer D, Ramshaw C. Carbon dioxide absorption and desorption in aqueous monoethanolamine solutions in a rotating packed bed. Ind Eng Chem Res 2007;46:2823–33.
[7] Cheng H-H, Lai C-C, Tan C-S. Thermal regeneration of alkanolamine solutions in a rotating packed bed. Int J Greenh Gas Control 2013;16:206–16.
[8] Joel AS, Wang M, Ramshaw C, Oko E. Process analysis of intensified absorber for post-combustion CO_2 capture through modelling and simulation. Int J Greenh Gas Control 2014;21:91–100.
[9] Borhani TN, Oko E, Wang M. Process modelling, validation and analysis of rotating packed bed stripper in the context of intensified CO_2 capture with MEA. J Ind Eng Chem 2019;75:285–95.
[10] Im D, Jung H, Lee JH. Modeling, simulation and optimization of the rotating packed bed (RPB) absorber and stripper for MEA-based carbon capture. Comput Chem Eng 2020;143:107102.
[11] Kang JL, Sun K, Wong DSH, Jang SS, Tan CS. Modeling studies on absorption of CO_2 by monoethanolamine in rotating packed bed. Int J Greenh Gas Control 2014;25:141–50.
[12] Thiels M, Wong DSH, Yu CH, Kang JL, Jang SS, Tan CS. Modelling and design of carbon dioxide absorption in rotating packed bed and packed column. IFAC-PapersOnLine 2016;49:895–900.
[13] Joel AS, Wang M, Ramshaw C. Modelling and simulation of intensified absorber for post-combustion CO_2 capture using different mass transfer correlations. Appl Therm Eng 2015;74:47–53.
[14] Borhani TN, Oko E, Wang M. Process modelling and analysis of intensified CO_2 capture using monoethanolamine (MEA) in rotating packed bed absorber. J Clean Prod 2018;204:1124–42.
[15] Oko E, Wang M, Ramshaw C. Study of mass transfer correlations for rotating packed bed columns in the context of solvent-based carbon capture. Int J Greenh Gas Control 2019;91:102831.
[16] Cortes Garcia GE, van der Schaaf J, Kiss AA. A review on process intensification in HiGee distillation. J Chem Technol Biotechnol 2017;92:1136–56.
[17] Agarwal L, Pavani V, Rao DP, Kaistha N. Process intensification in HiGee absorption and distillation: design procedure and applications. Ind Eng Chem Res 2010;49:10046–58.
[18] Chambers HH, Wall RG. Some factors affecting the design of centrifugal gas absorbers. Trans Instn Chem Engrs 1954;32:96–107.
[19] Joel AS, Wang M, Ramshaw C, Oko E. Modelling, simulation and analysis of intensified regenerator for solvent-based carbon capture using rotating packed bed technology. Appl Energy 2017;203:11–25.
[20] Luo Y, Chu GW, Zou HK, Wang F, Xiang Y, Shao L, et al. Mass transfer studies in a rotating packed bed with novel rotors: chemisorption of CO_2. Ind Eng Chem Res 2012;51:9164–72.
[21] Rao DP, Bhowal A, Goswami PS. Process intensification in rotating packed beds (HIGEE): an appraisal. Ind Eng Chem Res 2004;43:1150–62.
[22] Chen YS, Liu HS. Absorption of VOCs in a rotating packed bed. Ind Eng Chem Res 2002;41:1583–8.
[23] Luo Y, Chu GW, Zou HK, Zhao ZQ, Dudukovic MP, Chen JF. Gas-liquid effective interfacial area in a rotating packed bed. Ind Eng Chem Res 2012;51:16320–5.
[24] Llerena-Chavez H, Larachi F. Analysis of flow in rotating packed beds via CFD simulations—dry pressure drop and gas flow maldistribution. Chem Eng Sci 2009;64:2113–26.
[25] Watson KM. Thermodynamics of the liquid state: generalized prediction of properties. Ind Eng Chem 1943;35:398–406.
[26] Chilton TH, Colburn AP. Mass transfer (absorption) coefficients: prediction from data on heat transfer and fluid friction. Ind Eng Chem 1934;26:1183–7.
[27] Kvamsdal HM, Jakobsen JP, Hoff KA. Dynamic modeling and simulation of a CO_2 absorber column for post-combustion CO_2 capture. Chem Eng Process Process Intensif 2009;48:135–44.
[28] Aboudheir A, Tontiwachwuthikul P, Chakma A, Idem R. Kinetics of the reactive absorption of carbon dioxide in high CO_2-loaded, concentrated aqueous monoethanolamine solutions. Chem Eng Sci 2003;58:5195–210.
[29] Chen YS. Correlations of mass transfer coefficients in a rotating packed bed. Ind Eng Chem Res 2011;50:1778–85.
[30] Onda K, Takeuchi H, Okumoto Y. Mass transfer coefficients between gas and liquid phases in packed columns. J Chem Eng Japan 1968;1:56–62.
[31] Tung H-H, Mah RSH. Modeling liquid mass transfer in HIGEE separation process. Chem Eng Commun 1985;39:147–53.
[32] Billet R, Schultes M. Prediction of mass transfer columns with dumped and arranged packings. Chem Eng Res Des 1999;77:498–504.
[33] Burns JR, Jamil JN, Ramshaw C. Process intensification: operating characteristics of rotating packed beds — determination of liquid hold-up for a high-voidage structured packing. Chem Eng Sci 2000;55:2401–15.
[34] Nakagaki T, Isogai H, Sato H, Arakawa J. Updated e-NRTL model for high-concentration MEA aqueous solution by regressing thermodynamic experimental data at high temperatures. Int J Greenh Gas Control 2019;82:117–26.
[35] Gabrielsen J, Michelsen ML, Stenby EH, Kontogeorgis GM. A model for estimating CO2 solubility in aqueous alkanolamines. Ind Eng Chem Res 2005;44:3348–54.
[36] Ying J, Eimer DA, Wenjuan Y. Measurements and correlation of physical solubility of carbon dioxide in (monoethanolamine + water) by a modified technique. Ind Eng Chem Res 2012;51:6958–66.
[37] Rackett HG. Equation of state for saturated liquids. J Chem Eng Data 1970;15:514–7.
[38] Aspentech. Aspen physical property systems-physical property methods and models 11.1 2015:1–436.
[39] Horvath AL. Handbook of aqueous electrolyte solutions: Physical properties, estimation and correlation methods. Chichester: Ellis Horwood; 1985.
[40] Agbonghae EO, Hughes KJ, Ingham DB, Ma L, Pourkashanian M. A semi-empirical model for estimating the heat capacity of aqueous solutions of alkanolamines for CO_2 capture. Ind Eng Chem Res 2014;53:8291–301.
[41] Harun N. Dynamic simulation of MEA absorption process for CO_2 capture from power plants. University of Waterloo; 2012. PhD Thesis,.
[42] Ying J, Eimer DA. Measurements and correlations of diffusivities of nitrous oxide and carbon dioxide in monoethanolamine + water by laminar liquid jet. Ind Eng Chem Res 2012;51:16517–24.
[43] Fuller EN, Schettler PD, Giddings JC. A new method for prediction of binary gas-phase diffusion coefficients. Ind Eng Chem 1966;58:18–27.
[44] Singh SP, Counce RM, Wilson JH, Villiers-Fisher JF, Jennings HL, Lucero AJ, et al. Removal of volatile organic compounds from groundwater using a rotary air stripper. Ind Eng Chem Res 1992;31:574–80.
[45] Agbonghae EO, Hughes KJ, Ingham DB, Ma L, Pourkashanian M. Optimal process design of commercial-scale amine-based CO_2 capture plants. Ind Eng Chem Res 2014;53:14815–29.
[46] Otitoju O, Oko E, Wang M. A new method for scale-up of solvent-based post-combustion carbon capture process with packed columns. Int J Greenh Gas Control 2020;93:102900.
[47] Luo X, Wang M. Improving prediction accuracy of a rate-based model of an MEA-based carbon capture process for large-scale commercial deployment. Engineering 2017;3:232–43.
[48] Otitoju O, Oko E, Wang M. Technical and economic performance assessment of post-combustion carbon capture using piperazine for large scale natural gas combined cycle power plants through process simulation. Appl Energy 2021;292:116893.
[49] Gudena K, Rangaiah GP, Lakshminarayanan S. HiGee stripper-membrane system for decentralized bioethanol recovery and purification. Ind Eng Chem Res 2013;52:4572–85.

[50] Sudhoff D, Leimbrink M, Schleinitz M, Górak A, Lutze P. Modelling, design and flexibility analysis of rotating packed beds for distillation. Chem Eng Res Des 2015; 94:72–89.
[51] Canepa R, Wang M, Biliyok C, Satta A. Thermodynamic analysis of combined cycle gas turbine power plant with post-combustion CO_2 capture and exhaust gas recirculation. Proc Inst Mech Eng Part E J Process Mech Eng 2013;227:89–105.
[52] IEA-GHG. CO_2 capture in low-rank coal power plant. IEA Greenh Gas R&D Program Rep No2006/1; 2006.
[53] Lukin I, Pietzka L, Groß K, Górak A, Schembecker G. Economic evaluation of rotating packed bed use for aroma absorption from bioreactor off-gas. Chem Eng Process - Process Intens 2020;154:108011.
[54] Sheng M, Xie C, Zeng X, Sun B, Zhang L, Chu G, et al. Intensification of CO_2 capture using aqueous diethylenetriamine (DETA) solution from simulated flue gas in a rotating packed bed. Fuel 2018;234:1518–27.